Optics Communications 574 (2025) 131071

Contents lists available at ScienceDirect

Optics Communications

journal homepage: www.elsevier.com/locate/optcom

Investigation on the pressure broadening of ^{85}Rb $5S_{1/2}$–$5D_{3/2}$ monochromatic two–photon transition spectrum by multiple fluorescence detection

Wanwan Cao, Sandan Wang, Jinpeng Yuan *, Lirong Wang **, Liantuan Xiao, Suotang Jia

State Key Laboratory of Quantum Optics and Quantum Optics Devices, Institute of Laser Spectroscopy, Shanxi University, 92 Wucheng Road, Taiyuan 030006, China

Collaborative Innovation Center of Extreme Optics, Shanxi University, 92 Wucheng Road, Taiyuan 030006, China

ARTICLE INFO

Keywords:
Monochromatic two–photon transition spectrum
Pressure broadening
Multiple fluorescence detection

ABSTRACT

Precision measurement of spectral pressure broadening and full–width at half–maximum (FWHM) is essential for optimizing the performance of atomic clocks. Here, we experimentally demonstrate the ^{85}Rb $5S_{1/2}$ – $5D_{3/2}$ Doppler–free two–photon transition through a virtual level by using a 778 nm single laser. The high signal–to–noise ratio (SNR) $5S_{1/2}$ $(F = 2)$ – $5D_{3/2}$ $(F'' = 1, 2, 3, 4)$ monochromatic two–photon transition fluorescence spectra with 795 nm, 762 nm, and 420 nm are observed clearly simultaneously. Moreover, the impact of temperature on fluorescence spectral intensity and linewidth was thoroughly investigated. The pressure broadening of 40 ± 0.54 kHz/mTorr is obtained while the full–width at half–maximum of ~1.03 MHz is measured for the ^{85}Rb $5S_{1/2}$ $(F = 2)$ – $5D_{3/2}$ $(F'' = 4)$ transition spectrum. Finally, the effects of the laser power and the laser polarization combinations on the fluorescence spectra are investigated to obtain the optimal experimental parameters. This work paves the way for realizing a frequency standard in quantum communication of the C–band window.

1. Introduction

Precision measurement of atomic spectroscopy has immeasurable application prospects in the determination of fundamental physical constants [1,2], exploration of physics beyond the standard model [3–9], and improvement of atomic clocks performance [10–13]. Particularly, spectral pressure broadening measurement offers invaluable insights for analyzing systematic effects in atomic clocks, which play indispensable roles in geodesy [14,15], fundamental physics testing [16–19], and gravitational–wave detection [20]. One of the most straightforward and elegant methods for the high–resolution measurement of spectral pressure broadening relies on Doppler–free two–photon transition of atoms to eliminate the Doppler effect due to the atomic thermal motion in gas cell [21–23].

Recently, the $5S_{1/2}$ – $5D_{3/2}$ two–photon transition spectrum of the rubidium atoms has attracted tremendous attention for metrological application [24,25]. Several experimental platforms are developed for the rubidium $5S_{1/2}$ – $5D_{3/2}$ two–photon transition spectroscopy by two laser beams coupling with the real energy levels [26–30]. Additionally, the $5S_{1/2}$ – $5D_{3/2}$ two–photon transition spectrum of the rubidium atoms is achieved by a 778 nm single laser through a virtual energy level [31–33]. The ^{85}Rb $5S_{1/2}$ – $5D_{3/2}$ monochromatic two–photon transition spectrum has the advantages of superior Doppler–free background [34], relatively narrow natural linewidth (~0.97 MHz) [30], and relatively low sensitivity to the external environment, which provides a frequency standard candidate for a frequency–doubled 1556 nm laser in the C–band window for quantum telecommunication [26,35].

The ^{85}Rb $5S_{1/2}$ – $5D_{3/2}$ two–photon transition spectrum is obtained generally by detecting the 420 nm fluorescence generated by the decay cascade from the $5D_{3/2}$ to the $5S_{1/2}$ states via the $6P$ levels. The absolute transition frequency of rubidium $5S_{1/2}$ – $5D_{3/2}$ is measured by detecting the 420 nm monochromatic two–photon transition fluorescence spectra utilizing the continuous wave laser [31] or the femtosecond optical frequency comb [32]. Furthermore, the $5S_{1/2}$ – $5D_{3/2(5/2)}$ monochromatic two–photon transition fluorescence spectra are obtained by detecting 762 nm and 776 nm infrared light produced by $5D$ – $5P$ spontaneous radiation, which is increased by nearly two

* Corresponding author.
** Corresponding author at: State Key Laboratory of Quantum Optics and Quantum Optics Devices, Institute of Laser Spectroscopy, Shanxi University, 92 Wucheng Road, Taiyuan 030006, China.
E-mail addresses: yjp@sxu.edu.cn (J. Yuan), wlr@sxu.edu.cn (L. Wang).

https://doi.org/10.1016/j.optcom.2024.131071
Received 28 June 2024; Received in revised form 1 September 2024; Accepted 3 September 2024
Available online 5 September 2024

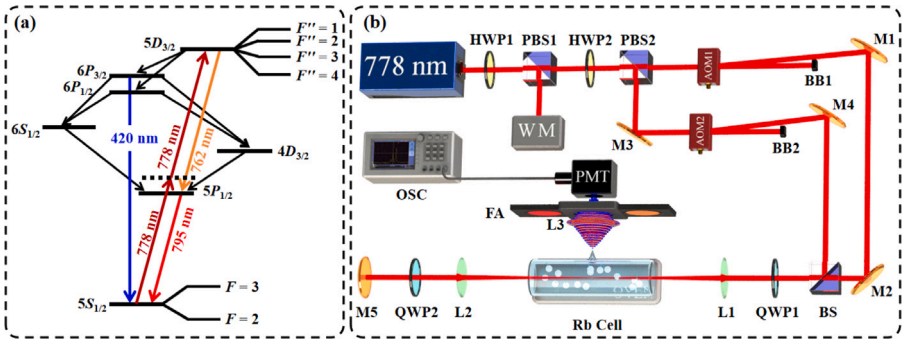

Fig. 1. (a) Energy–level diagram of ^{85}Rb $5S_{1/2} - 5D_{3/2}$ two–photon transition. (b) Schematic view of the experimental setup. HWP, half–wave plate; PBS, polarization beam splitter; WM, wavelength meter; AOM, acousto–optic modulator; M, high–reflection mirror; BS, beam splitter; QWP, quarter–wave plate; L, lens; FA, interference filter array; PMT, photomultiplier tube; OSC, oscilloscope.

orders of magnitude compared with 420 nm fluorescence [33]. A portable clock based on the $5S_{1/2} - 5D_{5/2}$ two–photon transition in rubidium is manufactured by detecting 776 nm fluorescence [13]. To the best of our knowledge, precision measuring the spectral pressure broadening of ^{85}Rb $5S_{1/2} - 5D_{3/2}$ two–photon transition has not been explored by simultaneously detecting 795 nm, 762 nm, and 420 nm fluorescence for compact Rubidium atomic clock analysis.

In this work, the spectral pressure broadening of ^{85}Rb $5S_{1/2} - 5D_{3/2}$ transition is studied by multiple fluorescence detection. The high signal–to–noise ratio (SNR) full fluorescence spectra of ^{85}Rb $5S_{1/2}$ $(F = 2) - 5D_{3/2}$ $(F'' = 1, 2, 3, 4)$ monochromatic two–photon transition are demonstrated experimentally by using a 778 nm single laser. The obtained 795 nm, 762 nm, and 420 nm fluorescence intensity ratios are consistent with the theoretical decay transition path branching ratios of $5D_{3/2} - 5P_{1/2}$, $5P_{1/2} - 5S_{1/2}$, and $6P_{1/2(3/2)} - 5S_{1/2}$, respectively. Furthermore, the changes of fluorescence spectral intensity and linewidth were studied at different temperatures. The pressure broadening of 40 ± 0.54 kHz/mTorr and full–width at half–maximum (FWHM) of ∼1.03 MHz is measured for the ^{85}Rb $5S_{1/2}$ $(F = 2) - 5D_{3/2}$ $(F'' = 4)$ transition spectrum. Finally, the dependency of $5S_{1/2} - 5D_{3/2}$ two–photon transition intensity on the laser power and the polarization combination of the laser beams are explored in detail. The precision measurement of spectral pressure broadening provides an excellent experimental platform for building up a frequency standard in quantum network and optical communication.

2. Experimental setup

The energy level diagram for ^{85}Rb $5S_{1/2} - 5D_{3/2}$ two–photon transition is shown in Fig. 1(a). The $5S_{1/2}$ ground state atoms are excited via a virtual level to the $5D_{3/2}$ excited state by using a single 778 nm laser, which is labeled by a dotted line in Fig. 1(a). The fluorescence generated directly from the unstable $5D_{3/2}$ excited state by spontaneous decay is the 762 nm, 776 nm, 5037 nm, and 5241 nm with branching ratio of 0.51, 0.11, 0.32, and 0.06, respectively [36]. In this process, the $5D_{3/2}$ state atoms will spontaneously radiate to the $5S_{1/2}$ ground state via several pathways with 795 nm, 762 nm, and 420 nm fluorescence emission. The 795 nm fluorescence with the highest branching ratios of 0.732 is emitted by $5P_{1/2} - 5S_{1/2}$, which comes from the cascade decay paths of $5D_{3/2} - 5P_{1/2} - 5S_{1/2}$, $5D_{3/2} - 6P_{1/2} - 4D_{3/2} - 5P_{1/2} - 5S_{1/2}$, $5D_{3/2} - 6P_{3/2} - 4D_{3/2} - 5P_{1/2} - 5S_{1/2}$, $5D_{3/2} - 6P_{1/2} - 6S_{1/2} - 5P_{1/2} - 5S_{1/2}$, and $5D_{3/2} - 6P_{3/2} - 6S_{1/2} - 5P_{1/2} - 5S_{1/2}$, respectively. The 762 nm fluorescence with branching ratio of 0.510 arises from the $5D_{3/2} - 5P_{1/2}$ decay. The 420 nm fluorescence with branching ratio of 0.105 is generated by the spontaneously radiate of $5D_{3/2}$ through $6P_{1/2} - 5S_{1/2}$ and $6P_{3/2} - 5S_{1/2}$ pathways, respectively [36]. The intensity of the fluorescence radiation is proportional to the population of $5D_{3/2}$ excited state atoms. Therefore, the 795 nm, 762 nm, and 420 nm fluorescence spectra can be measured synchronously to characterize the ^{85}Rb $5S_{1/2} - 5D_{3/2}$ two–photon transition intensity.

A schematic diagram of the experimental setup is shown in Fig. 1(b). The laser source is provided by an external cavity diode laser (Toptica, DL pro) with the wavelength of 778 nm, which is utilized to excite the ^{85}Rb $5S_{1/2} - 5D_{3/2}$ monochromatic two–photon transition. The laser beam is split into two components with the combination of a half wave plate (HWP1) and a polarization beam splitter (PBS1). One beam is employed to monitor the laser frequency using a wavelength meter (WS–7, HighFinesse). The other beam is again divided into two parts by the combination of HWP2 and PBS2 to excite the ^{85}Rb $5S_{1/2} - 5D_{3/2}$ transition. The transmitted beam is sent to the acousto–optic modulator (AOM1) with shifted frequency of $f_1 = 80$ MHz. The reflected beam passes through the AOM2 to achieve the frequency shift of $f_2 = 89.3$ MHz. The two beams with a frequency difference of $\Delta f = f_2 - f_1 = 9.3$ MHz are combined through a beam splitter (BS) for the interaction between laser and atoms. The frequency reference standard is established using frequency tuning technology. Two counter–propagating laser beams induced by a high reflector (M5) are applied to Rb vapor 2.5 cm in diameter and 10 cm in length to counteract the Doppler broadening. The temperature of the Rb vapor is measured by a thermocouple thermometer and then accurately controlled at specific value by a self–feedback system. Two lenses with a focal length of 20 cm (L1 and L2) are used to ensure that the waist of the focused laser beams in the middle of the cell is ∼100 μm. The generated 795 nm, 762 nm, and 420 nm fluorescence is focused through a lens with a focal length of 3 cm (L3) and passes through an interference filter array (FA) to resist the background noise caused by the scattered laser. The FA is composed of three 10 nm bandwidth bandpass filters with a central wavelength of 800 nm, 760 nm, and 420 nm (Thorlabs FB800–10, FBH760–10, FBH420–10), respectively. The generated 795 nm, 762 nm, and 420 nm fluorescence signal are detected synchronously by a side–window photomultiplier tube (PMT) (Hamamatsu, CR131). Finally, the monochromatic two–photon transition fluorescence spectra with 795 nm, 762 nm, and 420 nm are monitored by the oscilloscope (OSC).

3. Results and discussion

Fig. 2 shows the monochromatic two–photon transition fluorescence spectra of ^{85}Rb $5S_{1/2}$ $(F = 2) - 5D_{3/2}$ $(F'' = 1, 2, 3, 4)$ detected by PMT. These spectra are obtained by scanning the frequency of 778 nm laser, and the linewidths of the spectra are primarily determined by the linewidth of the laser itself. The fluorescence spectra are obtained under the condition that the laser power is 50 mW, the temperature of the Rb vapor is fixed at 150 °C, and the two counter–propagation beams have same linear polarization. The plotted fluorescence intensities have been corrected for filters transmission and the PMT response rate of different wavelength. The dots are experimental results, and the black lines are the multi–peak fitting results

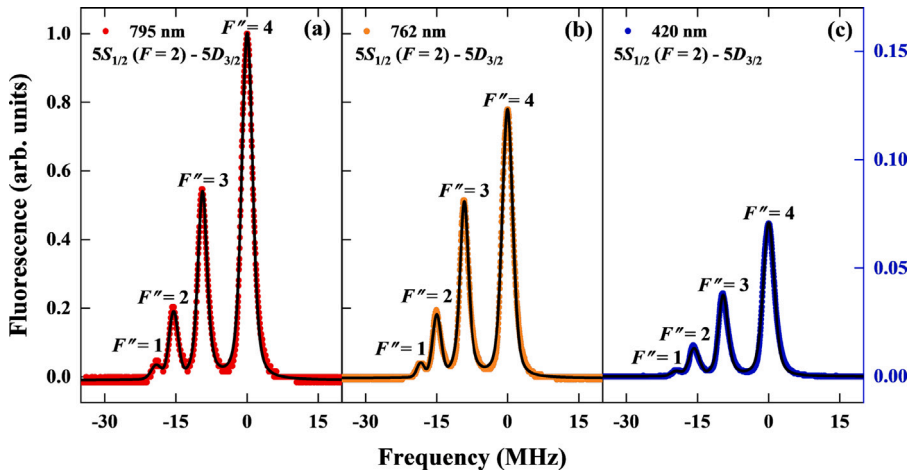

Fig. 2. The fluorescence spectra of ^{85}Rb $5S_{1/2}$ (F = 2) − $5D_{3/2}$ (F'' = 1, 2, 3, 4) monochromatic two−photon transition with (a) 795 nm, (b) 762 nm, and (c) 420 nm. The dots represent experimental results, and the black lines are multi−peak fitting curves with a Voigt function.

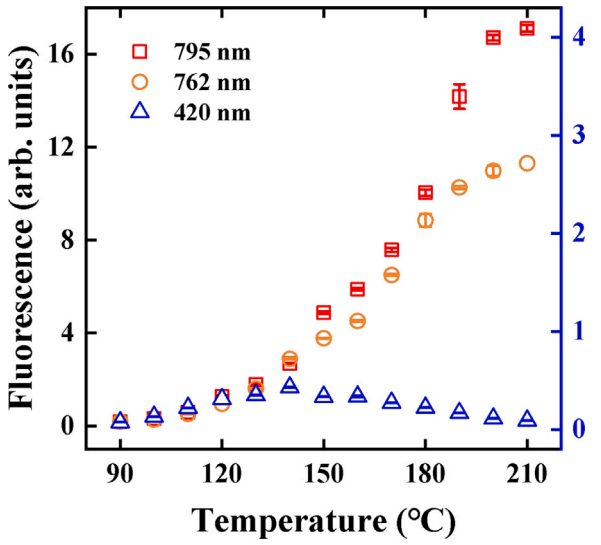

Fig. 3. The fluorescence intensities of ^{85}Rb $5S_{1/2}$ (F = 2) − $5D_{3/2}$ (F'' = 4) monochromatic two−photon transition with 795 nm, 762 nm, and 420 nm at various Rb vapor temperature. The errors are the standard deviation of three measurements.

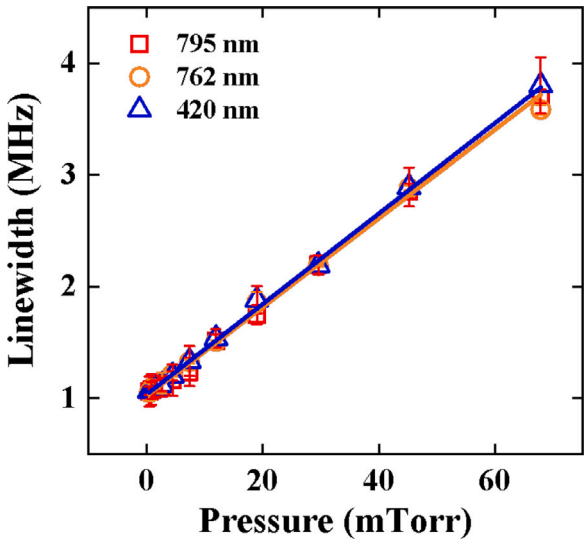

Fig. 4. The dependence of the ^{85}Rb $5S_{1/2}$ (F = 2) − $5D_{3/2}$ (F'' = 4) two−photon transition fluorescence spectra linewidths on the pressure of Rb vapor cell. The dots represent experimental results, and the solid lines are the linear fitting results. The errors are the standard deviation of three measurements.

with the Voigt profiles. The linear axis in Fig. 2 is designed to more accurately represent the relationship between fluorescence spectral intensities at different wavelengths, while still reflecting the spectral SNR. Each hyperfine splitting of the $5D_{3/2}$ state is well resolved with the fluorescence spectra of 795 nm, 762 nm, and 420 nm, as shown in Fig. 2 (a) − (c). Meanwhile, the peak intensity ratios of ^{85}Rb $5S_{1/2}$ (F = 2) − $5D_{3/2}$ (F'' = 4) hyperfine transition with the 795 nm, 762 nm, and 420 nm fluorescence are 1 : 0.8 : 0.07, respectively, which is a slight difference with the theoretical decay transition path branching ratios of 1 : 0.7 : 0.14 due to the reabsorption effect of the ground state atoms on the 795 nm and 420 nm fluorescence [36]. The simultaneous detection of ^{85}Rb $5S_{1/2}$ − $5D_{3/2}$ two−photon transition full fluorescence spectra with 795 nm, 762 nm, and 420 nm all reflect the atomic population of the $5D_{3/2}$ state perfectly. Three experimental parameters, the vapor temperature, the laser power, and the polarization combination of the laser beams, play a crucial role in obtaining accurate pressure broadening and narrow FWHM of the ^{85}Rb $5S_{1/2}$ − $5D_{3/2}$ two−photon transition spectrum.

The fluorescence intensities of ^{85}Rb $5S_{1/2}$ (F = 2) − $5D_{3/2}$ (F'' = 4) monochromatic two−photon transition with 795 nm, 762 nm, and 420 nm at different vapor temperatures are shown in Fig. 3. The temperature is increased from 90 to 210 °C while the laser power is kept at 50 mW. It can be observed that the fluorescence intensities of 795 nm (red dots) and 762 nm (orange dots) increase with the vapor temperature, which is attributed to the increasing atomic density. The fluorescence intensity of 795 nm is much higher than that of 762 nm when the temperature is higher than 190 °C because of the collision energy transfer influence [33]. When the vapor temperature is higher than 200 °C, the fluorescence intensities of 795 nm and 762 nm remain constant for the collisional broadening effect [33,37]. In addition, the 420 nm fluorescence intensity (blue dots) shows the trend of weak−strong−weak with the increasing vapor temperature due to the self−absorption effect of $6P - 5S_{1/2}$ transition [38]. Meanwhile, the 420 nm fluorescence intensity reaches the highest value when the vapor temperature is 140 °C, which is smaller than the 795 nm and 762 nm fluorescence intensity at the same temperature. This is because the 420 nm fluorescence has the smallest decay transition path branching ratios in the ^{85}Rb $5S_{1/2}$ − $5D_{3/2}$ monochromatic two−photon transition process.

The pressure broadening reveals the yet unknown dependence of broadening coefficients and the vapor temperature for the $5D_{3/2}$ hyperfine level. Meanwhile, the spectral FWHM can be calibrated by measuring pressure broadening, which is crucial to the frequency standard based on ^{85}Rb $5S_{1/2} - 5D_{3/2}$ two–photon transitions. Fig. 4 shows the linewidths (the Lorentzian part of the Voigt fit) of ^{85}Rb $5S_{1/2}$ ($F = 2$) $- 5D_{3/2}$ ($F'' = 4$) two–photon transition fluorescence spectra with 795 nm, 762 nm, and 420 nm as a function of the Rb vapor pressure (p). The temperature of the Rb vapor is adjusted from 100 to 210 °C while the power of the laser is kept at 50 mW. The expression of $\log_{10} p = 2.881 + 4.312 - 4040/T$ [39] is used to convert temperature (T) to ^{85}Rb vapor pressure (p). The linewidths of the fluorescence spectra with 795 nm, 762 nm, and 420 nm increase linearly with the increasing vapor pressure. The difference of the fluorescence spectra linewidths comes from the different spectral SNR. The linear fitting with a slope of 40 ± 0.54 kHz/mTorr and zero pressure–intercept of 1.03 ± 0.1 MHz are consistent with the experimental results. Therefore, the FWHM of the ^{85}Rb $5S_{1/2} - 5D_{3/2}$ transition spectrum with ~1.03 MHz is obtained, which is slightly higher than the natural linewidth of the $5D_{3/2}$ state (~0.97 MHz) because the contributions of transit–time broadening, the laser linewidth, and residual Doppler broadening arising from laser beams misalignment.

The two–photon transition peak intensity from the ground state $|5S_{1/2}F\rangle$ to the excited state $|5D_{3/2}F''\rangle$ can be characterized by [40, 41]:

$$P(5S_{1/2}F, 5D_{3/2}F'') \propto \left(\frac{1}{2F+1}\right) \frac{I_1 I_2}{\left[\omega_{5S_{1/2}F:5D_{3/2}F''} - (\omega_1 + k_1 \cdot v) - (\omega_2 + k_2 \cdot v)\right]^2 + \left(\frac{\gamma_{5D_{3/2}}}{2}\right)^2} \times \sum_{M_F,\ M_{F''}} \left| \sum_{F',\ M_{F'}} \frac{\langle 5D_{3/2}F''M''_F \mid \hat{e_2} \cdot d \mid 5P_{3/2}F'M'_F \rangle \langle 5P_{3/2}F'M'_F \mid \hat{e_1} \cdot d \mid 5S_{1/2}FM_F \rangle}{\omega_{5S_{1/2}F:5P_{3/2}F'} - (\omega_1 + k_1 \cdot v) - i\frac{\gamma_{5P_{3/2}}}{2}} \right|^2 \tag{1}$$

where I_1 and I_2 are the intensities of two counter–propagating beams that used to excite the two–photon process, F, F', and F'' are total atomic angular momentum quantum numbers, ω_1 and ω_2 are the two photon frequencies, k_1 and k_2 are the wave vectors, v is the atomic velocity, $\hat{e}_1$ and $\hat{e}_2$ are the unit vector along the quantization axis direction for the two laser beams, d is the electric dipole operator, γ_{nL} is the homogeneous linewidth of the $|nL_J\rangle$ state, and M_F, M'_F, and M''_F are the magnetic quantum numbers.

The fluorescence intensities of ^{85}Rb $5S_{1/2}$ ($F = 2$) $- 5D_{3/2}$ ($F'' = 4$) monochromatic two–photon transition with 795 nm, 762 nm, and 420 nm are characterized by varying the laser power, which is shown in Fig. 5. The experiment is conducted with the same condition of Fig. 2, except that the laser power increases from 30 to 70 mW. It is clearly shown that the fluorescence intensity increases with an increasing laser power and exhibits a quadratic relationship, which is depicted in the inset of Fig. 5. For the monochromatic two–photon transition with two counter–propagating laser beams, the laser intensity of two beams is the same ($I_1 = I_2$), therefore, the two–photon transition intensity has a linear relationship with the squared laser power from formula (1). In addition, the fluorescence intensity ratios of 795 nm, 762 nm, and 420 nm with 1 : 0.8 : 0.07 are consistent with the ^{85}Rb $5S_{1/2}$ ($F = 2$) $- 5D_{3/2}$ ($F'' = 4$) hyperfine transition peak intensity ratios of Fig. 2, indicating that the reabsorption effect of the $5S_{1/2}$ ground state atoms does not depend on the laser power. Although the fluorescence intensities of 795 nm, 762 nm, and 420 nm are different under the constant power, the same trend strongly verifies the proportional relationship between the fluorescence intensity and the square of laser power.

The fluorescence intensity of ^{85}Rb $5S_{1/2} - 5D_{3/2}$ two–photon transition also depends on the polarization combination of the laser beams. The Zeeman sublevels transition of $\Delta m_F = 0$, 1, −1 are driven by the π linearly polarized, σ^+ right–handed circularly polarized, and σ^- left–handed circularly polarized beams, respectively [42]. Fig. 6 illustrates the 795 nm, 762 nm, and 420 nm fluorescence intensities with different polarization angles of the reflected beam. Two quarter–wave plates (QWP1 and QWP2) are inserted into the experimental setup to control the polarization combination of the laser beams. The QWP1 is fixed in the path of the laser beam before the Rb vapor cell to obtain a circularly polarized beam. The QWP2 is located between the vapor cell and the M5 to control the polarization of the reflected beam from 0° to 180° with 10° intervals. The other experimental parameters are the same as the Fig. 2. It can be found that the 795 nm, 762 nm, and 420 nm fluorescence intensities all reach the minimum value when the counter–propagating beams are oppositely circularly polarization combination (QWP2 = 0°, 90°, and 180°) while the fluorescence intensities reach the maximum value with the same polarization combination

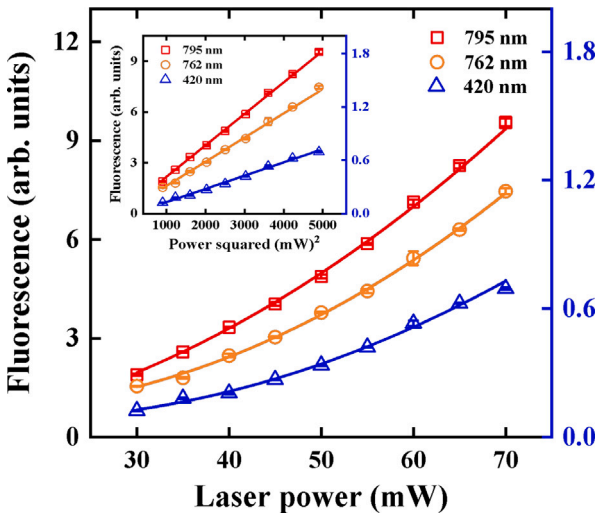

Fig. 5. The fluorescence intensities of ^{85}Rb $5S_{1/2}$ ($F = 2$) $- 5D_{3/2}$ ($F'' = 4$) monochromatic two–photon transition with 795 nm, 762 nm, and 420 nm as a function of laser power. The inset is the relationship between fluorescence intensity and the squared total laser power (P^2). The dots represent experimental results, and the solid lines are the theoretical fitting results. The errors are the standard deviation of three measurements.

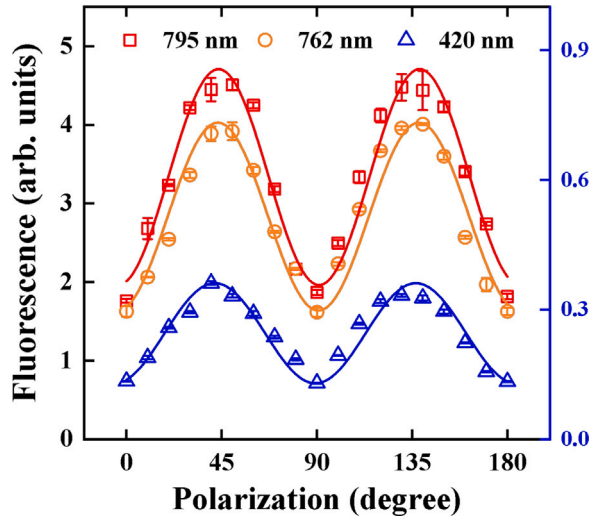

Fig. 6. The 795 nm, 762 nm, and 420 nm fluorescence intensities of ^{85}Rb $5S_{1/2}$ ($F = 2$) $- 5D_{3/2}$ ($F'' = 4$) monochromatic two–photon transition with different polarization combination of the laser beams. The dots represent experimental results, and the solid lines refer to fitting by the sine curve. The errors are the standard deviation of three measurements.

(QWP2 = 45° and 135°). These experimental results are consistent with the theoretical prediction that the polarization combination of $\sigma^+ - \sigma^-$ has lower probability and the polarization combination of $\sigma^+ - \sigma^+$ causes the highest transition probability [43,44]. Meanwhile, the fluorescence intensity ratios of 795 nm, 762 nm, and 420 nm with different laser polarization combinations agree well with the ^{85}Rb $5S_{1/2}$ $(F = 2) - 5D_{3/2}$ $(F'' = 4)$ hyperfine transition peak intensity ratios of Fig. 2. Similarly, the relationship between two−photon transition intensity and laser polarization combinations is verified strongly by the full fluorescence spectra with 795 nm, 762 nm, and 420 nm.

4. Conclusion

In summary, the spectral pressure broadening of ^{85}Rb $5S_{1/2} - 5D_{3/2}$ transition is investigated by multiple fluorescence detection. The high SNR full fluorescence spectra of ^{85}Rb $5S_{1/2}$ $(F = 2) - 5D_{3/2}$ $(F'' = 1, 2, 3, 4)$ monochromatic two−photon transition are demonstrated experimentally by using a 778 nm single laser. The obtained 795 nm, 762 nm, and 420 nm fluorescence intensity ratios are consistent with the theoretical decay transition path branching ratios of $5D_{3/2} - 5P_{1/2}$, $5P_{1/2} - 5S_{1/2}$, and $6P_{1/2(3/2)} - 5S_{1/2}$, respectively. The dependence of fluorescence intensities on the vapor temperature is investigated, which is directly related to the atomic density and vapor pressure. Then, the pressure broadening of 40 ± 0.54 kHz/mTorr is obtained while the full−width at half−maximum of ~1.03 MHz is measured for the ^{85}Rb $5S_{1/2}$ $(F = 2) - 5D_{3/2}$ $(F'' = 4)$ two−photon transition spectrum. A quadratic relationship between the laser power and fluorescence intensities with 795 nm, 762 nm, and 420 nm is observed, which is agree well with the theoretical prediction. The relationship between fluorescence intensities and laser beams polarization combinations obviously depends on the atomic transition selection rule. The infrared fluorescence intensity detection with high decay transition path branching ratios is an attractive alternative for achieving compact optical clocks based on ^{85}Rb $5S_{1/2} - 5D_{3/2}$ monochromatic two−photon transition.

CRediT authorship contribution statement

Wanwan Cao: Conceptualization, Data curation, Formal analysis, Methodology, Writing – original draft, Writing – review & editing. **Sandan Wang:** Conceptualization, Writing – original draft, Writing – review & editing. **Jinpeng Yuan:** Conceptualization, Methodology, Resources. **Lirong Wang:** Conceptualization, Methodology, Resources. **Liantuan Xiao:** Conceptualization, Funding acquisition. **Suotang Jia:** Conceptualization, Resources.

Declaration of competing interest

The authors declare that they have no known competing financial interests or personal relationships that could have appeared to influence the work reported in this paper.

Data availability

Data will be made available on request.

Acknowledgments

This work is supported by the Innovation Program for Quantum Science and Technology, China (2023ZD0300902), the National Natural Science Foundation of China (62075121, 12474359, 62475136), Fundamental Research Program of Shanxi Province, China (20240302121 1158), the Fund Program for the Scientific Activities of Selected Returned Overseas Professionals in Shanxi Province, China (2023001), Shanxi Scholarship Council of China (2024−003), the Fund for Postdoctoral Fellowship Program of CPSF, China (GZC20231510) and the Fund for Shanxi "1331 Project", China.

References

[1] A. Beyer, L. Maisenbacher, A. Matveev, R. Pohl, K. Khabarova, A. Grinin, T. Lamour, D.C. Yost, T.W. Hänsch, N. Kolachevsky, T. Udem, The Rydberg constant and proton size from atomic hydrogen, Science 358 (6359) (2017) 79–85, http://dx.doi.org/10.1126/science.aah6677.

[2] A. Grinin, A. Matveev, D.C. Yost, L. Maisenbacher, V. Wirthl, R. Pohl, T.W. Hänsch, T. Udem, Two-photon frequency comb spectroscopy of atomic hydrogen, Science 370 (6520) (2020) 1061–1066, http://dx.doi.org/10.1126/science.abc7776.

[3] C.J. Kennedy, E. Oelker, J.M. Robinson, T. Bothwell, D. Kedar, W.R. Milner, G.E. Marti, A. Derevianko, J. Ye, Precision metrology meets cosmology: Improved constraints on ultralight dark matter from atom-cavity frequency comparisons, Phys. Rev. Lett. 125 (20) (2020) 201302, http://dx.doi.org/10.1103/PhysRevLett.125.201302.

[4] C. Solaro, S. Meyer, K. Fisher, J.C. Berengut, E. Fuchs, M. Drewsen, Improved isotope-shift-based bounds on bosons beyond the standard model through measurements of the $^2D_{3/2} - ^2D_{5/2}$ interval in Ca^+, Phys. Rev. Lett. 125 (12) (2020) 123003, http://dx.doi.org/10.1103/PhysRevLett.125.123003.

[5] I. Counts, J. Hur, D.P. Aude Craik, H. Jeon, C. Leung, J.C. Berengut, A. Geddes, A. Kawasaki, W. Jhe, V. Vuletić, Evidence for nonlinear isotope shift in Yb^+ search for new boson, Phys. Rev. Lett. 125 (12) (2020) 123002, http://dx.doi.org/10.1103/PhysRevLett.125.123002.

[6] N. Figueroa, J. Berengut, V. Dzuba, V. Flambaum, D. Budker, D. Antypas, Precision determination of isotope shifts in ytterbium and implications for new physics, Phys. Rev. Lett. 128 (7) (2022) 073001, http://dx.doi.org/10.1103/PhysRevLett.128.073001.

[7] J. Yuan, W. Yang, M. Jing, H. Zhang, Y. Jiao, W. Li, L. Zhang, L. Xiao, S. Jia, Quantum sensing of microwave electric fields based on Rydberg atoms, Rep. Progr. Phys. 86 (10) (2023) 106001, http://dx.doi.org/10.1088/1361-6633/acf22f.

[8] Z. Zhang, R. Wang, Y. Zhang, Y.V. Kartashov, F. Li, H. Zhong, H. Guan, K.-L. Gao, F. Li, Y. Zhang, M. Xiao, Observation of edge solitons in photonic graphene, Nature Commun. 11 (2019) http://dx.doi.org/10.1038/s41467-020-15635-9.

[9] J. Wu, M. Guo, H. Zhou, J. Liu, J. Li, J. Zhang, Experimental realization of efficient nondegenerate four-wave mixing in cesium atoms, Opt. Express 30 (8) (2022) 12576, http://dx.doi.org/10.1364/oe.452790.

[10] A.D. Ludlow, M.M. Boyd, J. Ye, E. Peik, P.O. Schmidt, Optical atomic clocks, Rev. Modern Phys. 87 (2) (2015) 637, http://dx.doi.org/10.1103/RevModPhys.87.637.

[11] B. Rahaman, S. Dutta, Hyperfine coupling constants of the cesium $7D_{5/2}$ state measured up to the octupole term, Opt. Lett. 47 (18) (2022) 4612–4615, http://dx.doi.org/10.1364/ol.469086.

[12] B. Rahaman, S. Dutta, High-precision measurement of the hyperfine splitting and ac Stark shift of the $7d^2\ D_{3/2}$ state in atomic cesium, Phys. Rev. A 106 (4) (2022) 042811, http://dx.doi.org/10.1103/PhysRevA.106.042811.

[13] R. Beard, K.W. Martin, J.D. Elgin, B.L. Kasch, S.P. Krzyzewski, Two-photon rubidium clock detecting 776 nm fluorescence, Opt. Express 32 (5) (2024) 7417–7425, http://dx.doi.org/10.1364/OE.513974.

[14] W. McGrew, X. Zhang, R. Fasano, S. Schäffer, K. Beloy, D. Nicolodi, R. Brown, N. Hinkley, G. Milani, M. Schioppo, et al., Atomic clock performance enabling geodesy below the centimetre level, Nature 564 (7734) (2018) 87–90, http://dx.doi.org/10.1038/s41586-018-0738-2.

[15] J. Grotti, S. Koller, S. Vogt, S. Häfner, U. Sterr, C. Lisdat, H. Denker, C. Voigt, L. Timmen, A. Rolland, et al., Geodesy and metrology with a transportable optical clock, Nat. Phys. 14 (5) (2018) 437–441, http://dx.doi.org/10.1038/s41567-017-0042-3.

[16] M. Takamoto, I. Ushijima, N. Ohmae, T. Yahagi, K. Kokado, H. Shinkai, H. Katori, Test of general relativity by a pair of transportable optical lattice clocks, Nature Photonics 14 (7) (2020) 411–415, http://dx.doi.org/10.1038/s41566-020-0619-8.

[17] N. Huntemann, B. Lipphardt, C. Tamm, V. Gerginov, S. Weyers, E. Peik, Improved limit on a temporal variation of m_p / m_e from comparisons of Yb^+ and Cs atomic clocks, Phys. Rev. Lett. 113 (21) (2014) 210802, http://dx.doi.org/10.1103/PhysRevLett.113.210802.

[18] R. Godun, P. Nisbet-Jones, J. Jones, S. King, L. Johnson, H. Margolis, K. Szymaniec, S. Lea, K. Bongs, P. Gill, Frequency ratio of two optical clock transitions in $^{171}Yb^+$ and constraints on the time variation of fundamental constants, Phys. Rev. Lett. 113 (21) (2014) 210801, http://dx.doi.org/10.1103/physrevlett.113.210801.

[19] J. Yuan, H. Zhang, C. Wu, G. Chen, L. Wang, L. Xiao, S. Jia, Creation and control of vortex-beam arrays in atomic vapor, Laser Photonics Rev. 17 (2023) http://dx.doi.org/10.1002/lpor.202200667.

[20] S. Kolkowitz, I. Pikovski, N. Langellier, M.D. Lukin, R.L. Walsworth, J. Ye, Gravitational wave detection with optical lattice atomic clocks, Phys. Rev. D 94 (12) (2016) 124043, http://dx.doi.org/10.1103/physrevd.94.124043.

[21] F. Biraben, B. Cagnac, G. Grynberg, Experimental evidence of two-photon transition without Doppler broadening, Phys. Rev. Lett. 32 (12) (1974) 643, http://dx.doi.org/10.1103/PHYSREVLETT.32.643.

[22] T.W. Hänsch, S.A. Lee, R. Wallenstein, C. Wieman, Doppler-free two-photon spectroscopy of hydrogen $1S - 2S^*$, Phys. Rev. Lett. 34 (6) (1975) 307, http://dx.doi.org/10.1142/9789812813787_0002.
[23] B. Rahaman, S.C. Wright, S. Dutta, Observation of quantum interference of optical transition pathways in Doppler-free two-photon spectroscopy and implications for precision measurements, Phys. Rev. A 109 (4) (2024) 042820, http://dx.doi.org/10.1103/PhysRevA.109.042820.
[24] T. Udem, R. Holzwarth, T.W. Hänsch, Optical frequency metrology, Nature 416 (6877) (2002) 233–237, http://dx.doi.org/10.1038/416233a.
[25] S. Koller, J. Grotti, S. Vogt, A. Al-Masoudi, S. Dörscher, S. Häfner, U. Sterr, C. Lisdat, Transportable optical lattice clock with 7×10^{-17} uncertainty, Phys. Rev. Lett. 118 (7) (2017) 073601, http://dx.doi.org/10.1103/PhysRevLett.118.073601.
[26] C. Gabbanini, F. Ceccherini, S. Gozzini, A. Lucchesini, Resonance-enhanced ionization spectroscopy of laser-cooled rubidium atoms, Meas. Sci. Technol. 10 (9) (1999) 772, http://dx.doi.org/10.1088/0957-0233/10/9/302.
[27] N. Prajapati, Z. Niu, I. Novikova, Quantum-enhanced two-photon spectroscopy using two-mode squeezed light, Opt. Lett. 46 (8) (2021) 1800–1803, http://dx.doi.org/10.1364/OL.418398.
[28] A. Chakrabarti, A. Ray, Exploring hyperfine levels of non-Rydberg excited states in a Ξ system using Autler–Townes splitting, Appl. Opt. 59 (3) (2020) 735–741, http://dx.doi.org/10.1364/ao.381321.
[29] R. Cardman, X. Han, J.L. MacLennan, A. Duspayev, G. Raithel, Ac polarizability and photoionization-cross-section measurements in an optical lattice, Phys. Rev. A 104 (6) (2021) 063304, http://dx.doi.org/10.1103/physreva.104.063304.
[30] Z. Xu, M. Cai, S. You, S. Zhang, H. Liu, Optical-optical double resonance spectroscopy of Rb $5D_{3/2,5/2}$ in magnetic fields, Spectrochim. Acta Part B: Atom. Spectrosc. 193 (2022) 106453, http://dx.doi.org/10.1016/j.sab.2022.106453.
[31] F. Nez, F. Biraben, R. Felder, Y. Millerioux, Optical frequency determination of the hyperfine components of the $5S_{1/2} - 5D_{3/2}$ two-photon transitions in rubidium, Opt. Commun. 102 (5–6) (1993) 432–438, http://dx.doi.org/10.1016/0030-4018(93)90417-4.
[32] O. Terra, Absolute frequency measurement of the hyperfine structure of the $5S_{1/2} - 5D_{3/2}$ two-photon transition in rubidium using femtosecond frequency comb, Measurement 144 (2019) 83–87, http://dx.doi.org/10.1016/j.measurement.2019.04.042.
[33] K. Hassanin, P. Federsel, F. Karlewski, C. Zimmermann, $5S - 5D$ Two-photon transition in rubidium vapor at high densities, Phys. Rev. A 107 (4) (2023) 043104, http://dx.doi.org/10.1103/PhysRevA.107.043104.
[34] H. Moon, W. Lee, L. Lee, J. Kim, Double resonance optical pumping spectrum and its application for frequency stabilization of a laser diode, Appl. Phys. Lett. 85 (18) (2004) 3965–3967, http://dx.doi.org/10.1063/1.1813629.
[35] S. Wang, J. Yuan, L. Wang, L. Xiao, S. Jia, Investigation on the monochromatic two-photon transition spectroscopy of rubidium by using intensity modulation method, J. Phys. Soc. Japan 87 (8) (2018) 084301, http://dx.doi.org/10.7566/JPSJ.87.084301.
[36] O. Heavens, Radiative transition probabilities of the lower excited states of the alkali metals, JOSA 51 (10) (1961) 1058–1061, http://dx.doi.org/10.1364/JOSA.51.001058.
[37] M. Baranger, Simplified quantum-mechanical theory of pressure broadening, Phys. Rev. 111 (2) (1958) 481, http://dx.doi.org/10.1103/PHYSREV.111.481.
[38] O. Terra, H. Hussein, An ultra-stable optical frequency standard for telecommunication purposes based upon the $5S_{1/2} - 5D_{5/2}$ two-photon transition in Rubidium, Appl. Phys. B 122 (2016) 1–12, http://dx.doi.org/10.1007/s00340-015-6309-4.
[39] D.A. Steck, Rubidium 87 D line data, 2001, URL https://steck.us/alkalidata/.
[40] J.E. Stalnaker, S. Chen, M. Rowan, K. Nguyen, T. Pradhananga, C. Palm, D.J. Kimball, Velocity-selective direct frequency-comb spectroscopy of atomic vapors, Phys. Rev. A 86 (3) (2012) 033832, http://dx.doi.org/10.1103/PhysRevA.86.033832.
[41] S.-D. Wang, J.-P. Yuan, L.-R. Wang, L.-T. Xiao, S.-T. Jia, Investigation on the Cs $6S_{1/2}$ to $7D$ electric quadrupole transition via monochromatic two-photon process at 767 nm, Front. Phys. 16 (2021) 1–6, http://dx.doi.org/10.1007/s11467-020-0988-y.
[42] K.D. Bonin, T.J. McIlrath, Two-photon electric-dipole selection rules, J. Opt. Soc. Am. B 1 (1) (1984) 52–55, http://dx.doi.org/10.1364/JOSAB.1.000052.
[43] S. Dai, W. Xia, Y. Zhang, J. Zhao, D. Zhou, Q. Wang, Q. Yu, K. Li, X. Qi, X. Chen, Polarization dependence of the direct two photon transitions of ^{87}Rb atoms by erbium: Fiber laser frequency comb, Opt. Commun. 378 (2016) 35–40, http://dx.doi.org/10.1016/j.optcom.2016.05.059.
[44] D. McGloin, M. Dunn, D. Fulton, Polarization effects in electromagnetically induced transparency, Phys. Rev. A 62 (5) (2000) 053802, http://dx.doi.org/10.1103/PHYSREVA.62.053802.